CrystEngComm

ROYAL SOCIETY OF CHEMISTRY

PAPER

View Article Online
View Journal | View Issue

Cite this: *CrystEngComm*, 2025, **27**, 2895

Understanding surface morphology evolution in magnetron sputtered AlN templates: mitigating tensile stress and enhancing crystal quality†

Li Jiang,[ab] Jianwei Ben,*[b] Ke Jiang,[b] Shanli Zhang,[b] Tong Wu,[b] Zikai Nie,[bd] Entao Zhang,[bc] Shunpeng Lu,[b] Xiaojuan Sun*[b] and Dabing Li*[abc]

Received 8th January 2025,
Accepted 11th March 2025

DOI: 10.1039/d5ce00027k

rsc.li/crystengcomm

The thickness and surface morphology of aluminum nitride (AlN) templates are crucial for evaluating their quality and suitability for device applications. However, the relationship between these two factors remains unclear for AlN templates grown *via* magnetron sputtering. This study systematically investigates the surface restructuring mechanisms in AlN films during thickness progression, revealing a stress-driven morphological transition. As film thickness increases, accumulated tensile stress exceeding ~0.5 GPa triggers the spontaneous formation of "flower-like" surface patterns through stress relief. While mitigating further stress buildup, this morphological transformation degrades crystalline quality post-high-temperature annealing. Through strategic optimization of sputtering thermodynamics, we successfully preset compressive stress in AlN films and extended the critical thickness for morphological degradation to 2 μm. The resulting high-quality thick AlN films exhibit simultaneously improved surface continuity and enhanced crystalline perfection. These results provide valuable insights into the stress-morphology interactions in sputtered AlN films, offering new strategies for optimizing AlN template growth and enhancing the performance of AlN-based devices.

Introduction

Aluminum nitride (AlN) as a kind of direct wide-band-gap semiconductor (6.2 eV) exhibits exceptional properties such as high thermal conductivity, high acoustic velocity, and strong polarization characteristics.[1–5] It is an ideal material for ultraviolet optoelectronic devices, microelectromechanical systems (MEMS), radio frequency (RF) devices, and surface acoustic wave (SAW) devices.[6–9] Furthermore, AlN is commonly used as a substrate for the epitaxial growth of other III–V compound semiconductors, broadening its range of applications. However, the fabrication of bulk single-crystal AlN remains challenging due to the high decomposition pressure of AlN. Consequently, most of the research has focused on the preparation of AlN films on heterogeneous substrates.[10–14]

The thickness and surface morphology of AlN films are critical, as they directly affect the electronic and optical properties of the material, thereby influencing device performance. For instance, in AlN-based SAW devices, film thickness and processing conditions play a significant role in determining frequency response, operational speed, and insertion loss.[15–17] Moreover, researchers have prepared AlN films with different surface structures by chemical vapor deposition (CVD), molecular beam epitaxy (MBE) and other methods. They found the structural variations significantly influence the physical and chemical properties of AlN by introducing defects, such as carbon (C) and oxygen (O) impurities and vacancies of aluminum (Al) and nitrogen (N).[18–20] Therefore, the ability to produce smooth AlN films with precise control over thickness is essential for optimizing the performance of the aforementioned devices.

Among the various fabrication methods, magnetron sputtering is one of the most widely adopted techniques, offering high uniformity and low impurity content. Extensive research has been conducted to investigate the surface evolution of AlN films fabricated by magnetron sputtering. Studies indicate that surface morphology, roughness, and other properties are sensitive to sputtering conditions, including temperature, nitrogen flow ratio, and sputtering

[a] *School of Microelectronics, University of Science and Technology of China, Hefei, Anhui 230026, People's Republic of China*
[b] *State Key Laboratory of Luminescence Science and Technology, Changchun Institute of Optics, Fine Mechanics and Physics, Chinese Academy of Sciences, Changchun 130033, China. E-mail: benjianwei@ciomp.ac.cn, sunxj@ciomp.ac.cn, lidb@ciomp.ac.cn*
[c] *University of Chinese Academy of Sciences, Beijing 100039, People's Republic of China*
[d] *School of Integrated Circuits, Dalian University of Technology, Dalian 116024, China*

† Electronic supplementary information (ESI) available. See DOI: https://doi.org/10.1039/d5ce00027k

power.[21–25] Researchers have also explored the effects on the crystal orientation, defects, and device performance of AlN films by adjusting magnetron sputtering parameters (substrate material, substrate angle, nitrogen ratio, sputtering power, *etc.*).[26–29] High *c*-axis-oriented AlN films have been successfully grown using unbalanced magnetron sputtering, which utilizes an asymmetric magnetic field to enhance ion bombardment. This approach facilitates the formation of denser grains, reduces surface roughness, and improves crystal quality.[30] Furthermore, film thickness plays a crucial role in determining the microstructure and defect characteristics of AlN films. Longer sputtering time increases the grain size and roughness. However, as film thickness increases, the AlN film becomes denser, with a gradual transition in orientation from disordered to well-ordered AlN (002) planes.[31,32] These findings emphasize the critical importance of controlling film thickness to enhance crystal quality and minimize defect density.

Despite these advancements, the mechanisms by which film thickness influences surface morphology evolution remain inadequately understood. In this work, we employ reactive magnetron sputtering to deposit AlN films and systematically investigates the relationship between film thickness and surface morphology evolution. It has been demonstrated that when the film thickness surpasses a critical threshold, a distinct "flower-like" morphology emerges, coinciding with stress relaxation within the film. This morphology increases surface roughness and degrades crystal quality due to elevated grain boundary content and defect density. The research further reveals that the critical thickness for the onset of "flower-like" morphology can be effectively increased from 800 nm to over 2 μm by raising the sputtering temperature from 650 °C to 750 °C. This temperature adjustment enhances film quality and surface smoothness, providing valuable insights into the interplay between stress and surface morphology.

Experimental procedure

AlN films were sputtered on *c*-plane sapphire substrates (*c*-plane off to *M*-axis 0.2°, single-side polished, surface roughness 0.119 nm) by reactive magnetron sputtering (iTops A230). A pure Al target (99.999%) and a sputtering power of 3000 W were used. AlN films with thickness from 200 nm to 2.5 μm were sputtered in $Ar:N_2$ (10% : 90%) mixed atmosphere at different temperatures (650 °C, 700 °C, 750 °C), the average growth rate of AlN growth at 650 °C, 700 °C, 750 °C are 0.2484 nm s^{-1}, 0.2437 nm s^{-1}, 0.2387 nm s^{-1}, respectively, which are similar.

High-resolution X-ray diffraction (XRD: D8 Discover) was used to characterize the crystal quality (dislocation density) of the AlN film. Scanning electron microscopy (SEM: S-4800) and atomic force microscopy (AFM: MULTIMODE 8) were used to characterize the surface morphology of the sample. Raman spectroscopy (Omni-λ3008i) was used to characterize the stress of the sample.

Results and discussion

To investigate the morphology evolution with the thickness of the AlN film, AlN films with varying thicknesses were grown. The surface morphology and thickness of the samples were characterized by SEM, and the results are shown in Fig. 1. Fig. 1(a)–(g) correspond to films with thicknesses of 200 nm, 500 nm, 800 nm, 1.1 μm, 1.4 μm, 2 μm, and 2.5 μm, respectively. In the samples with thicknesses between 200 nm and 500 nm, the typical columnar structure characteristic of magnetron sputtered AlN is observed. With the increase in film thickness, there is a gradual increase in the size of the columnar crystals. However, at the thickness of 800 nm, a "flower-like" morphology begins to appear on the surface, and the size of the columnar crystals no longer increases. The surface area covered by this "flower-like" morphology increases with film thickness, leading to the formation of a layered structure. Upon reaching a thickness of 2.5 μm, the entire surface of the AlN film is uniformly covered by the "flower-like" morphology. Fig. 1(h) shows the SEM image of the 2 μm sample taken at a 45°-tilt angle. The "flower-like" morphology exhibits a multi-layered architectural growth. The SEM results show that there is a clear relationship between the surface morphology of AlN and its thickness. Furthermore, the "flower-like" morphology usually occurs between the columnar crystals, as shown in the red squares in Fig. 1(c) and (d). The dotted squares in Fig. 1(c) and (d) are the enlarged images of the "flower-like" morphology marked in the solid squares. From the enlarged images, it can be seen that the "flower-like" structures are started at the grain boundaries. The two enlarged images in Fig. 1(d) demonstrate the process by which the "flower-like" morphology evolves from formation to enlargement.

The cross-sectional SEM shows that the "flower-like" morphology exhibits a conical structure, with the apex of the cone growing between the columnar crystals. The base of the cone starts approximately 800 nm to 1 μm away from the substrate, which is consistent with the critical thickness at which the "flower-like" morphology first appears. Moreover, all the conical structures have the similar apex angle, approximately 46° (half of the angle of the conical structure is about 23° ± 2°), as indicated in Fig. 1(e)–(g). To investigate whether the "flower-like" morphology corresponds to a special crystal orientation, the wide range (10–80°) XRD 2Theta-Omega measurements were performed on AlN samples with varying thicknesses as shown in Fig. S1.† It was found that there is only the peak of (0002) plane AlN for all the samples, although the "flower-like" morphology have fully covered the surface of AlN with 2 μm thickness. Additionally, AFM measurements were performed on samples with different thicknesses, revealing that the "flower-like" structures are about 40 nm higher than the columnar structures, with the center of the "flower-like" features being lower than the surrounding areas. The details are shown in Fig. S2.† Moreover, as the film thickness increases, the surface roughness also increases. The presence of "flower-

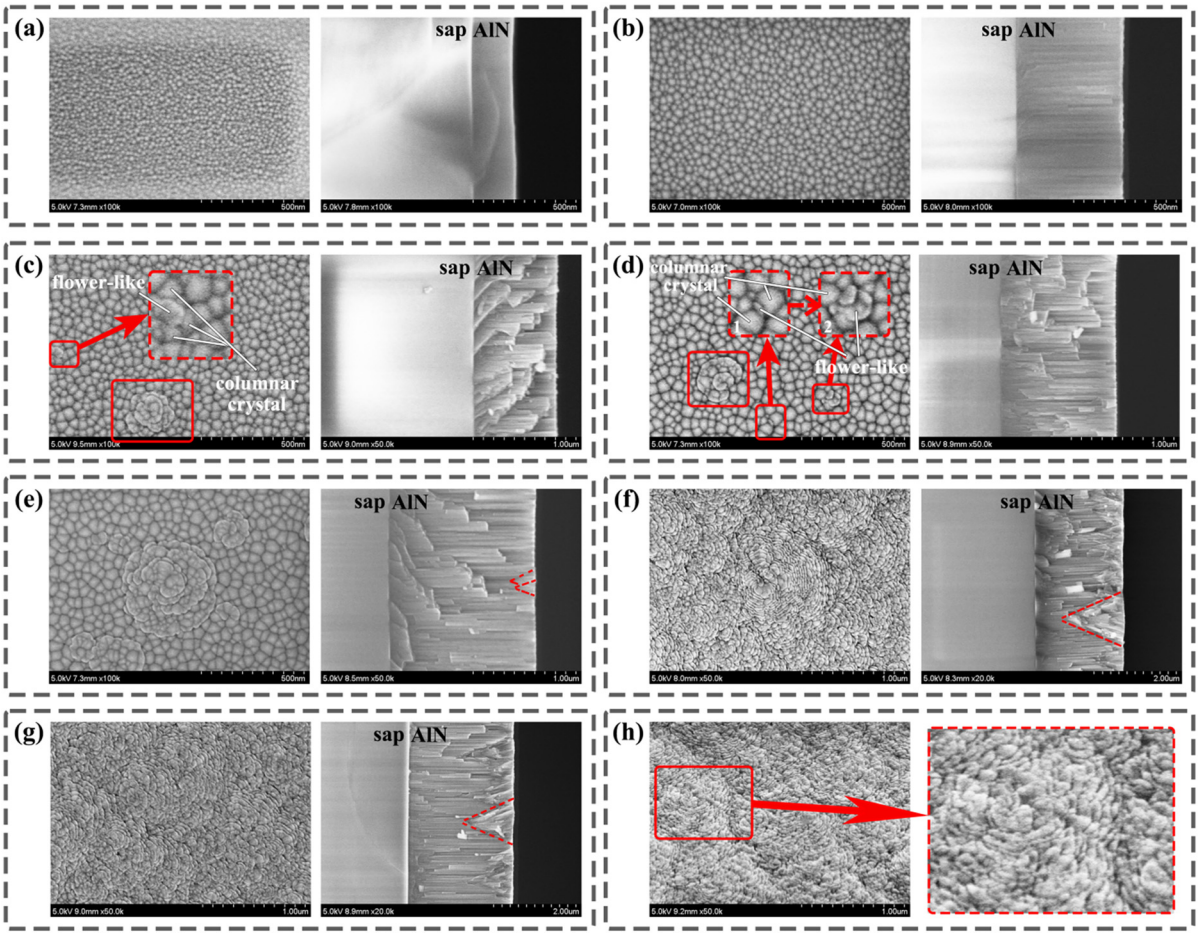

Fig. 1 SEM results of samples with different thicknesses. (a–g) Films with thicknesses of 200 nm, 500 nm, 800 nm, 1.1 μm, 1.4 μm, 2 μm, and 2.5 μm, respectively (the left side of each picture is the surface morphology, and the right side is the cross-sectional view). (h) 2.5 μm sample taken at 45°-tilt angle. In addition, the dotted squares in (c, d and h) are the zoomed-in view of the "flower-like" morphology in the solid squares.

like" morphology greatly increases the roughness of the surface. The surface roughness of samples with different thicknesses is listed in Table S1.†

From the surface characterization results shown in Fig. 1, it can be observed that as the thickness of sputtered AlN templates increases, the grain size generally increases. According to published research, the merging of columnar structures will introduce tensile stress to the film.[33] To investigate the stress of the samples with different thicknesses and morphologies, Raman measurements were used to characterize the stress. Since the surface morphology varies across different regions of the samples, Raman mapping was conducted to ensure the reliability of the stress results as exhibited in Fig. S3.† They present uniform stress

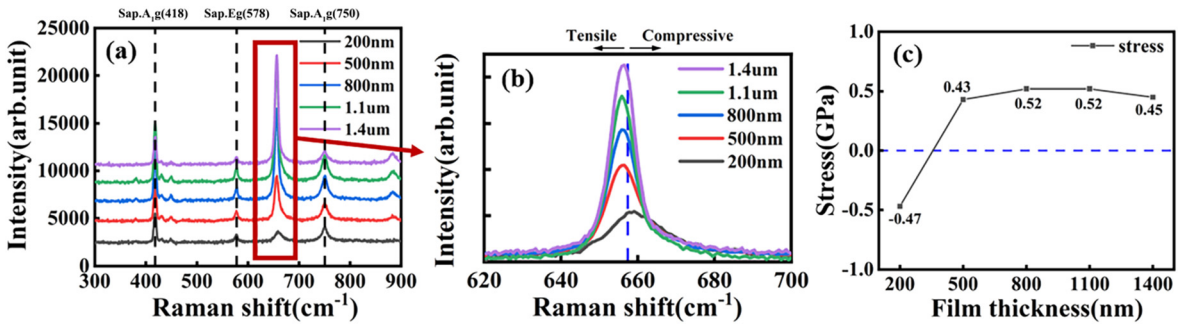

Fig. 2 (a) Raman spectra of samples with different thicknesses at the sputtering temperature of 650 °C (the dotted lines are the Raman peaks of sapphire). (b) Zoomed-in view of the AlN E_2(high) peak. (c) Stress situation of samples with different thicknesses at the sputtering temperature of 650 °C.

distribution throughout the AlN film, which can confirm the reliability of the stress characterization in Fig. 2. The Raman spectra for AlN samples of different thicknesses are shown in Fig. 2(a), with a zoomed-in view of the AlN E_2(high) peak shown in Fig. 2(b), because the E_2(high) peak is commonly used to calculate the stress in AlN films. As the film thickness increases, the peak position exhibits an initial redshift followed by stabilization. The stress magnitude can be calculated using the formula:[33]

$$\sigma_{xx} = \frac{\omega_{E_2(high)} - 657.4}{k} \quad (1)$$

in which, ω = 657.4 cm^{-1} represents the E_2(high) peak position of AlN in its stress-free state, while k = 2.55 cm^{-1} GPa^{-1} is the biaxial stress coefficient, and the sign of σ_{xx} indicates the type of stress: positive for tensile stress and negative for compressive stress. The stress in AlN films of different thicknesses was calculated, as shown in Fig. 2(c). The results show that thinner films experience greater compressive stress. As the film thickness increases, tensile stress is induced. By comparing the SEM results of AlN films with different thicknesses (Fig. 1), with the increase in film thickness, the grain size of the AlN columnar structure increases gradually, and the grain merging process occurs. This leads to tensile stress accumulation, which is consistent with previous research.[33,34] When the film thickness surpasses 800 nm, the tensile stress stabilizes at approximately 0.5 GPa. Comprehensive analysis of the SEM images reveals that the accumulation of tensile stress eventually leads to the emergence of the characteristic "flower-like" surface morphology. This correspondence may suggest a potential link in stress-morphology interactions of sputtered AlN films. To further verify this phenomenon, repeat experiments were conducted; the results were consistent, and the details are shown in Fig. S4.† These experiments suggest that the appearance of the "flower-like" morphology on the AlN film surface is closely related to the stress variation. As the film thickness increases, tensile stress accumulates. When the film thickness surpasses a critical threshold, a distinct "flower-like" morphology emerges, which correlates with stress relaxation within the film. This morphological transition serves as a mechanism to alleviate stress.

To further investigate the interplay between surface morphology and stress, an experiment was designed with the goal of changing the stress state during film growth in order to control the surface morphology. During experiments, we found that the stress can be adjusted by changing the sputtering temperature. As shown in Fig. 3(a)–(c), as the temperature increased from 600 °C to 750 °C, the tensile stress of 200 nm AlN film decreased from 0.29 GPa to −2.35 GPa. Increasing the sputtering temperature can reduce the tensile stress (introduce compressive stress), resulting in a lower tensile stress in AlN films with the same thickness. This effectively increases the critical thickness of the threshold tensile stress and the appearance of "flower-like" morphology, enabling the growth of thicker AlN films with superior surface morphology. Therefore, we raised the sputtering temperature to 700 °C and grew AlN films of varying thicknesses. The surface morphology and stress variations of the samples were measured, with stress characterization

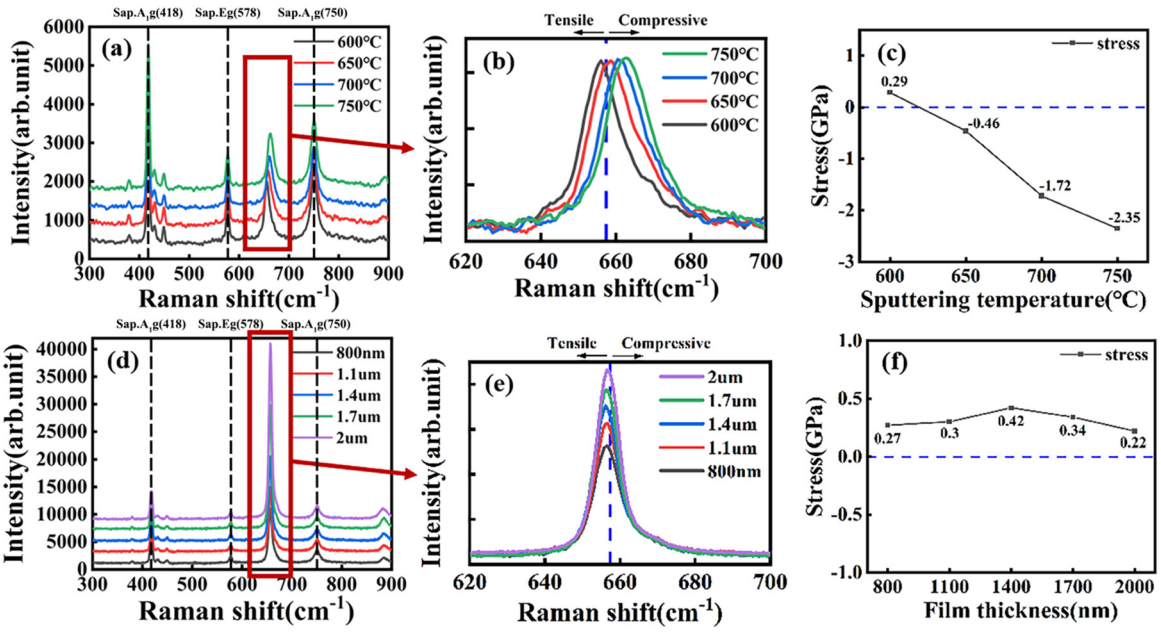

Fig. 3 (a) Raman spectra of 200 nm samples with different sputtering temperatures (the dotted lines are the Raman peaks of sapphire). (b) Enlarged view of the AlN E_2(high) peak in (a). (c) Stress situation of samples with different sputtering temperatures. (d) Raman spectra of samples with different thicknesses at the sputtering temperature of 700 °C (the dotted lines are the Raman peaks of sapphire). (e) Enlarged view of the AlN E_2(high) peak in (d). (f) Stress situation of samples with different thicknesses at the sputtering temperature of 700 °C.

results shown in Fig. 3(d)–(f). The tensile stress gradually increases for films with thicknesses ranging from 800 nm to 1.4 μm. However, beyond 1.4 μm, the tensile stress decreases, indicating a release of tensile stress. The critical thickness at which the stress reaches saturation was delayed to 1.4 μm. Fig. 4(a)–(e) show the SEM surface morphologies of samples with different thicknesses at 700 °C. The results indicate that the critical thickness for the appearance of the "flower-like" morphology increased to 1.4 μm, which corresponds to the critical thickness where the stress reaches a stable value. This validates the conclusion that the appearance of the "flower-like" morphology is due to the alleviation of the continuously accumulating tensile stress. By increasing the sputtering temperature to 750 °C, the critical thickness for morphological degradation can be further delayed from 1.4 μm to 2 μm. These results demonstrate that the stress state during the film growth process is one of the key factors influencing the surface morphology of the film.

High-temperature annealing (HTA) is considered an effective method for improving the crystallinity of AlN films.[35] In the process of HTA, the columnar domains will coalesce and the domain boundaries in AlN films annihilate, resulting in improved crystal quality.[36–38] To further investigate the influence of the "flower-like" morphology on the quality of AlN films with/without annealing, samples with the same thickness but different surface morphologies were selected for high-temperature face-to-face annealing (1700 °C in N_2 atmosphere under normal pressure for 1 h). One sample, exhibiting a "flower-like" morphology, was sputtered at 650 °C (as shown in Fig. 1(f)), while the other, without "flower-like" morphology, was sputtered at 750 °C (as shown in Fig. 4(f)). X-ray

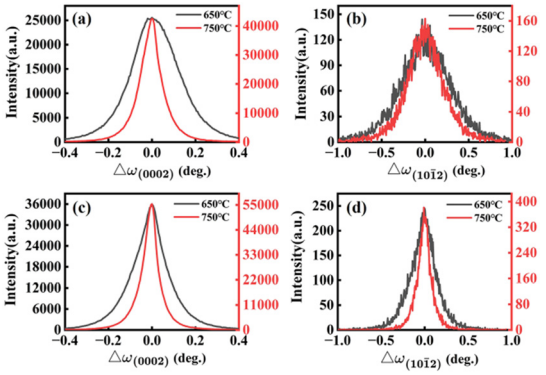

Fig. 5 XRC of the (0002) and (10–12) planes for 2 μm samples at different sputtering temperatures. (a and b) without annealing. (c and d) With 1700 °C annealing.

rocking curve (XRC) analysis was performed with and without annealing, and the results are shown in Fig. 5. With high-temperature annealing, the sample with "flower-like" morphology shows a reduction in the full width at half maximum (FWHM) of the X-ray rocking curve (XRC) for the (0002)/(10–12) planes from 810/1857.6 arcsec to 558/910.8 arcsec, those of the sample without "flower-like" morphology decrease from 399.6/1256.4 arcsec to 313.2/522 arcsec. These results indicate that the presence of the "flower-like" morphology negatively affects the quality of HTA-AlN films. Notably, the (0002) and (10–12) planes are associated with screw dislocations and edge dislocations, respectively. The screw dislocation density and edge dislocation density of AlN films are calculated as:[39,40]

$$\rho_s = \frac{\beta^2_{(0002)}}{2\pi \ln 2 \times |b_c|^2} \quad (2)$$

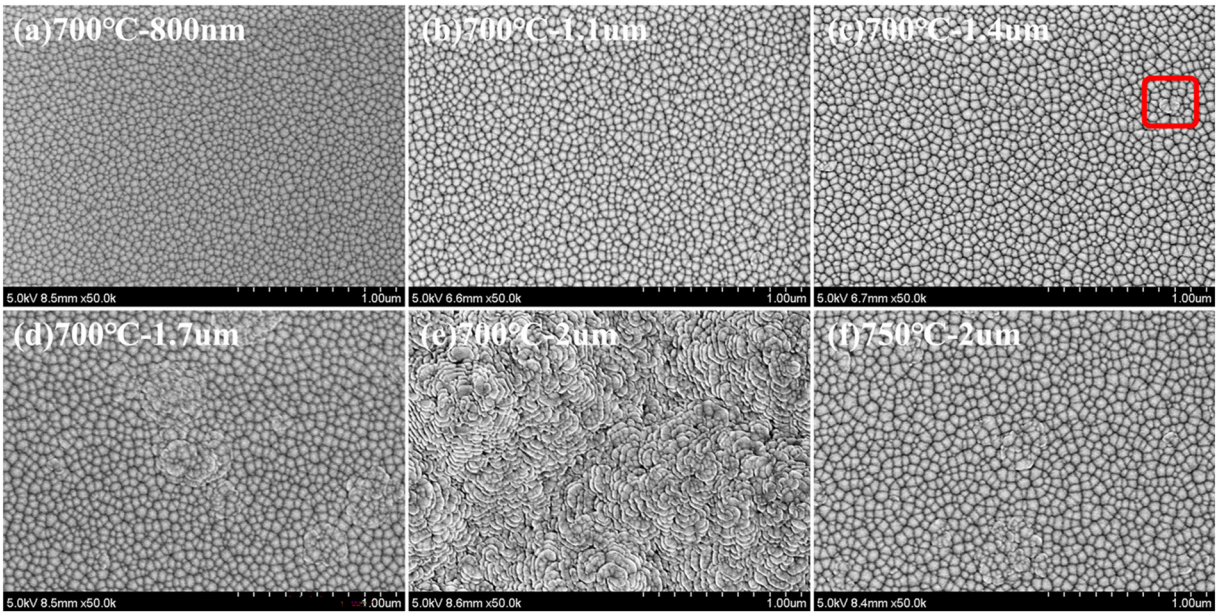

Fig. 4 SEM surface morphology of samples. (a–e) Films with thicknesses of 800 nm, 1.1 μm, 1.4 μm, 1.7 μm, and 2 μm at the sputtering temperature of 700 °C. (f) Film with thickness of 2 μm at the sputtering temperature of 750 °C.

$$\rho_e = \frac{\beta^2_{(10\bar{1}2)}}{2\pi \ln 2 \times |b_a|^2} \quad (3)$$

in which, ρ_s and ρ_e are the screw dislocation density and edge dislocation density, $\beta_{(0002)}$ and $\beta_{(10-12)}$ are the FWHM of the XRC obtained from testing on the (0002) and (10–12) planes, b_a and b_c are the Burgers vectors in the *c*-plane and perpendicular to the *c*-plane. Calculation results reveal that, for samples of the same thickness, the screw dislocation density of the sample without the "flower-like" morphology (3.47×10^8 cm^{-2}) without annealing is one order of magnitude lower than that of the sample with the "flower-like" morphology (1.43×10^9 cm^{-2}).

Fig. 6 shows the SEM surface and cross-sectional morphology of the two samples with annealing. The results indicate that numerous voids will appear in these two samples, which are consistent with previous research.[41] For HTA-AlN with "flower-like" morphology, the voids are located at the interfaces between the layers of the "flower-like" structure from the plane view of SEM, as shown in Fig. 6(a). The SEM cross-sectional view further highlights the conical arrangement of the voids, as indicated in Fig. 6(b). The largest voids are found at the outermost edges of the "flower-like" morphology, where they intersect with the columnar structure. The SEM plane and cross-sectional views of HTA-AlN without "flower-like" morphology are shown in Fig. 6(c) and (d), respectively. It can be found that in the HTA-AlN with "flower-like" morphology, the voids within the "flower-like" structures exhibit both larger dimensions and higher density compared to the HTA-AlN without "flower-like" morphology. Additionally, these voids are concentrated near the upper surface of the sample, particularly at the interface between the "flower-like" morphology and the columnar structure. According to the analysis of void formation mechanisms, it is understood that the generation of voids with high-temperature annealing in AlN films is primarily due to the high grain boundary density and defect density, which confirms that the material properties in the "flower-like" morphology are distinct from those in the columnar region. The multi-layer, conical structure of the "flower-like" morphology leads to a high concentration of grain boundaries, which promotes the formation of a large number of voids and defects with annealing. In addition, the initially better quality AlN before HTA do not lead to better quality HTA-AlN as discussed in Fig. S5,† which supporting the conclusion that the "flower-like" morphology is harmful to obtain high quality HTA-AlN films. Therefore, the presence of the "flower-like" morphology negatively impacts the film quality. The increased sputtering temperature reduces the film's tensile stress during growth, optimizing the surface morphology and simultaneously improving the crystalline quality of the film.

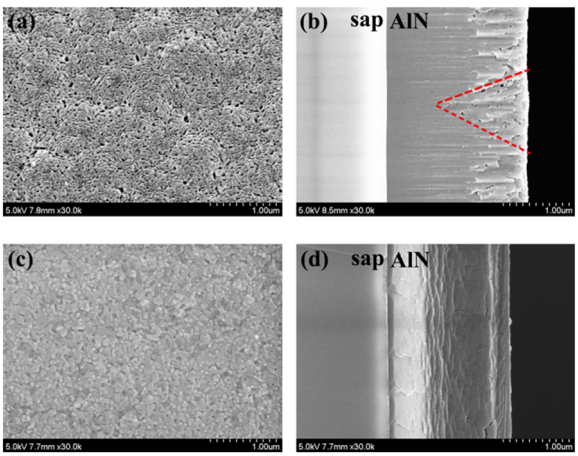

Fig. 6 SEM images of 2 μm samples with 1700 °C annealing. (a) Surface morphology and (b) cross-sectional SEM image of annealed AlN template sputtered at 650 °C. (c) Surface morphology and (d) cross-sectional SEM image of annealed AlN template sputtered at 750 °C.

Conclusions

This work deciphers the thickness-dependent morphological dynamics in magnetron-sputtered AlN films, revealing a stress-mediated self-organization mechanism. Progressive tensile stress accumulation during film growth triggers spontaneous "flower-like" surface restructuring at the critical thickness, serving as a stress-relief pathway. The formation of the "flower-like" structure deteriorates the HTA-AlN quality due to the persistence of high grain boundaries. Crucially, we demonstrate that thermodynamic regulation of sputtering conditions can preset compressive stress in AlN films and effectively postpone the degradation threshold to 2 μm. This research deepens the understanding of stress-morphology interactions in magnetron-sputtered AlN films and offers a pathway to the development of smooth and high-quality films for advanced device applications.

Data availability

Data supporting the findings of this study can be provided by contacting the corresponding author.

Author contributions

Li Jiang: conceptualization, data curation, formal analysis, investigation, methodology, validation, writing-original draft, writing-review & editing. Jianwei Ben: conceptualization, investigation, methodology, writing-review & editing. Ke Jiang, Shanli Zhang: formal analysis, resources, writing-review & editing. Tong Wu: data curation, investigation, writing-review & editing. Zikai Nie, Entao Zhang: investigation, writing-review & editing. Shunpeng Lu: formal analysis, writing-review & editing. Xiaojuan Sun, Dabing Li: mechanism analysis, supervision, writing-review & editing.

Conflicts of interest

There are no conflicts to declare.

Acknowledgements

National Key Research and Development Program of China (2023YFB3610300); National Natural Science Foundation of China (12234018, 62121005, U22A2084, 62204241); Youth Innovation Promotion Association of the Chinese Academy of Sciences (2023223); Natural Science Foundation of Jilin Province (20230101345JC, SKL202302026); Young Elite Scientist Sponsorship Program By CAST (YESS20200182).

Notes and references

1 S. Yamamoto, A. Tani and T. Gounji, *Jpn. J. Appl. Phys.*, 1989, **28**, 209.
2 M. Strassburg, J. Senawiratne, N. Dietz, U. Haboeck, A. Hoffmann, V. Noveski, R. Dalmau, R. Schlesser and Z. Sitar, *J. Appl. Phys.*, 2004, **96**, 5870.
3 A. Ababneh, U. Schmid, J. Hernando, J. L. Sánchez-Rojas and H. Seidel, *Mater. Sci. Eng., B*, 2010, **172**, 253.
4 T. Kamohara, M. Akiyama and N. Kuwano, *Appl. Phys. Lett.*, 2008, **92**, 093506.
5 W. Guo, J. Xie, C. Akouala, S. Mita, A. Rice, J. Tweedie, I. Bryan, R. Collazo and Z. Sitar, *J. Cryst. Growth*, 2013, **366**, 20.
6 Z. Lu, F. Wang and Y. Liu, *Sci. Rep.*, 2021, **11**, 12720.
7 T. A. Growden, W. Zhang, E. R. Brown, D. F. Storm, D. J. Meyer and P. R. Berger, *Light: Sci. Appl.*, 2018, **7**, 17150.
8 D. Y. Kim, J. H. Park, J. W. Lee, S. Hwang, S. J. Oh, J. Kim, C. Sone, E. F. Schubert and J. K. Kim, *Light: Sci. Appl.*, 2015, **4**, e263.
9 K. Jiang, X. Sun, Z. Shi, H. Zang, J. Ben, H. Deng and D. Li, *Light: Sci. Appl.*, 2021, **10**, 69.
10 M. Mansor, R. Norhaniza, A. Shuhaimi, M. I. Hisyam, A. Omar, A. Williams and M. R. M. Hussin, *Sci. Rep.*, 2023, **13**, 8793.
11 J. Wang, N. Xie, F. Xu, L. Zhang, J. Lang, X. Kang, Z. Qin, X. Yang, N. Tang, X. Wang, W. Ge and B. Shen, *Nat. Mater.*, 2023, **22**, 853.
12 A. L. Mulyo, M. K. Rajpalke, P. E. Vullum, H. Weman, K. Kishino and B. Fimland, *Sci. Rep.*, 2020, **10**, 853.
13 W. Wang, W. Yang, Y. Lin, S. Zhou and G. Li, *Sci. Rep.*, 2015, **5**, 16453.
14 S. Lu, J. Ben, K. Jiang, S. Zhang, R. Zhang, J. Hao, Z. Liu, W. Sun, Z. Nie, X. Sun and D. Li, *J. Semicond.*, 2025, **46**, 154.
15 M. Clement, L. Vergara, E. Iborra, A. Sanzhervas, J. Olivares and J. Sangrador, AlN-on-Si SAW filters: Influence of film thickness, IDT geometry and substrate conductivity, *Proc. IEEE Ultrasonics Symp.*, 2005, **4**, 1900.
16 O. Legrani, T. Aubert, O. Elmazria, A. Bartasyte, P. Nicolay, A. Talbi, P. Boulet, J. Ghanbaja and D. Mangin, *IEEE Trans. Ultrason. Ferroelectr. Freq. Control*, 2016, **63**, 898.
17 D. Phan and G. Chung, *Appl. Surf. Sci.*, 2011, **257**, 8696.
18 H. H. Nersisyan, J. Lee, H. Kim, S. Ryu and B. Yoo, *Int. Mater. Rev.*, 2019, **65**, 323.
19 F. Zhang, Q. Wu, X. Wang, N. Liu, J. Yang, Y. Hu, L. Yu, X. Wang, Z. Hu and J. Zhu, *J. Phys. Chem. C*, 2009, **113**, 4053.
20 L. Shen, W. Lv, N. Wang, L. Wu, D. Qi, Y. Ma and W. Lei, *CrystEngComm*, 2017, **19**, 5940.
21 Z. Wei, L. Shen, Y. Kuang, J. Wang, G. Yang and W. Lei, *J. Cryst. Growth*, 2024, **625**, 127439.
22 L. V. Baranova and V. I. Strunin, *J. Phys.: Conf. Ser.*, 2020, **1546**, 012110.
23 M. A. Moreira, I. Doi, J. F. Souza and J. A. Diniz, *Microelectron. Eng.*, 2011, **88**, 802.
24 B. Sundarapandian, A. Yassine, L. Kirste, M. Baeumler, P. Straňák, E. Fisslthaler, M. Prescher, M. Yassine, A. Nair, M. Raghuwanshi and O. Ambacher, *J. Appl. Phys.*, 2023, **134**, 185107.
25 S. Uchiyama, Y. Ishigami, M. Ohta, M. Niigaki, H. Kan, Y. Nakanishi and T. Yamaguchi, *J. Cryst. Growth*, 1998, **189**, 448.
26 J. Xiong, H. Gu, W. Wu, M. Hu, P. Du and H. Xie, *J. Electron. Mater.*, 2011, **40**, 1578.
27 J. Lee, J. Jung, M. Lee and J. Park, *Thin Solid Films*, 2004, **447**, 610.
28 X. Jiang, Y. Wu, J. Qi, Y. Liu, Y. Wang, J. Gao, H. Hei and S. Yu, *Vacuum*, 2024, **220**, 112829.
29 H. Cheng, *Thin Solid Films*, 2003, **425**, 85.
30 G. Ke, Y. Tao, Y. Lu, Y. Bian, T. Zhu, H. Guo and Y. Chen, *J. Alloys Compd.*, 2015, **646**, 446.
31 P. Limsuwan, N. Udomkan, S. Meejoo and P. Winotai, *Int. J. Mod. Phys. B*, 2005, **19**, 2073.
32 Y. Bian, M. Liu, G. Ke, Y. Chen, J. DiBattista, E. Chan and Y. Yang, *Surf. Coat. Technol.*, 2015, **267**, 65.
33 M. X. Wang, F. J. Xu, N. Xie, Y. H. Sun, B. Y. Liu, W. K. Ge, X. N. Kang, Z. X. Qin, X. L. Yang, X. Q. Wang and B. Shen, *Appl. Phys. Lett.*, 2019, **114**, 112105.
34 A. Stolz, A. Soltani, B. Abdallah, J. Charrier, D. Deresmes, P. Y. Jouan, M. A. Djouadi, E. Dogheche and J. C. De Jaeger, *Thin Solid Films*, 2013, **534**, 442.
35 Z. Nie, J. Ben, E. Zhang, X. Ma, S. Zhang, Z. Shi, S. Lu, K. Jiang, X. Sun and D. Li, *Rengong Jingti Xuebao*, 2023, **52**, 1016.
36 H. Miyake, C. Lin, K. Tokoro and K. Hiramatsu, *J. Cryst. Growth*, 2016, **456**, 155.
37 L. Zhao, K. Yang, Y. Ai, L. Zhang, X. Niu, H. Lv and Y. Zhang, *J. Mater. Sci.: Mater. Electron.*, 2018, **29**, 13766.
38 J. Ben, X. Sun, Y. Jia, K. Jiang, Z. Shi, H. Liu, Y. Wang, C. Kai, Y. Wu and D. Li, *CrystEngComm*, 2018, **20**, 4623.
39 J. Xiong, J. Tang, T. Liang, Y. Wang, C. Xue, W. Shi and W. Zhang, *Appl. Surf. Sci.*, 2010, **257**, 1161.
40 R. Chierchia, T. Böttcher, H. Heinke, S. Einfeldt, S. Figge and D. Hommel, *J. Appl. Phys.*, 2003, **93**, 8918.
41 S. Xiao, R. Suzuki, H. Miyake, S. Harada and T. Ujihara, *J. Cryst. Growth*, 2018, **502**, 41.